INVESTIGATION OF ARTIFICIAL METAMATERIALS AND MULTILAYER NANOCOMPOSITES IN EXTERNAL MAGNETIC FIELD

Plamen Dankov, Valda Levcheva

Faculty of Physics, Sofia University "St. Kliment Ohridski", 5 J. Bourchier blvd., 1164 Sofia, Bulgaria

Abstract

The modern multilayer nanomaterials and artificial metamaterials can change their dielectric and magnetic parameters (complex permittivity and permeability) in external magnetic and/or electric fields. This property has been known as magneto-electric effect: variation of dielectric constant in external dc magnetic field and v.v., variation of magnetic constant in external dc voltage. In this paper, we present the results for the observed magneto-electric effect in several types of materials including nanocomposites, multiferroics and artificial metamaterials in an external magnetic field applied in two directions: perpendicular and parallel to the sample surface. The measurement range of interest is 0.01-40 GHz. Some of the presented effects have been observed for the first time for the considered materials. Attempts to bind the observed effect with the sample chemical and physical structures have been described. These investigations are the first stage of a bigger project for complete characterization of artificial materials in external dc magnetic field.

Keywords: *composite materials, dielectric anisotropy, dielectric constant, magneto-electric effect, metamaterials, microwave measurements, multiferoics*

1. INTRODUCTION

Recently, the so-called magneto-electric materials appear among the modern artificial materials [1-4]. The common issue for these materials is the magneto-electric coupling; now, the complex electric and magnetic flux densities, $\vec{D}$ and $\vec{B}$, in the bi-anisotropic magneto-electric materials can be expressed as $\vec{D} = (\hat{\varepsilon})\vec{E} + (\hat{\xi})\vec{B}$ and $\vec{B} = (\hat{\mu})\vec{H} + (\hat{\zeta})\vec{E}$, where $(\hat{\varepsilon})$, $(\hat{\mu})$ are the permittivity and permeability tensors, while $(\hat{\xi})$, $(\hat{\zeta})$ are tensors of the corresponding magneto-electric (ME) coupling coefficients. When the parameters ε, μ, ξ, ζ are scalars, the materials become bi-isotropic. The above relations show that the equivalent permittivity ε_{eq} in such materials can depend not only on the response to the electric (E) field, but also on the response to the magnetic (H) field in the considered media (v.v. for equivalent permeability μ_{eq}).

Magnetoelectrics have attracted much attention namely for their ability to control magnetic behavior by applied dc voltage and/or electrical behavior by applied external magnetic field (i.e. by dc current). This property provides numerous advantages to integrate tunable composite components in tunable smart devices [5] such as magnetic field sensors, current sensors, energy harvesters, memory devices, filters, etc. [6, 7]. The so-called direct magnetoelectrics [8], in which the coupling between the magnetic and electric order is enforced by symmetry reasons, are rarely found in nature and the magnetoelectric effect they exhibit is relatively weak. However, the composite magnetoelectric materials, in which the ME coupling is indirect [1-3], show several orders stronger ME magnitude than in direct magnetoelectrics. Nowadays, there exist many new artificial materials with proven ME effect: solid-state or soft materials, amorphous materials, thin films, ME nanocomposites, powders, laminates, ME liquids, etc. [9-18]. The ME effect can be observed as at the room temperature, as well as at lower or higher temperature intervals [19].

In most of the cases, the ME effect in multiferoics has been characterized at relatively low frequencies; typically, up to several hundred MHz [20-24]. Only few papers consider characterization of this effect in the microwave range [25-27]. However, the existence of ME at higher frequencies provides numerous advantages to integrate these tunable composite components in the microwave devices [28-30]. The

characterization of the ME effect in the microwave ranges requires an optimized combination between two measurement schemes – the microwave setup for determination of the S parameters of the structure with incorporated magnetoelectric and the magnetic system for applying the external magnetic field [31] and they cannot influence each other.

In this paper, we describe our initial experimental investigations of the influence of applied dc external magnetic field over the dielectric and magnetic properties of a class of artificial materials with expectation that they may have ME properties in the microwave range. The main efforts have been directed to ME observation in multiferoics samples from Z-type hexaferrite $Sr_3Co_2Fe_{24}O_{41}$ [32] in external magnetic field (0-025T) in the frequency range 0.01-40 GHz. The used method is based on determination of the additional losses and phases in covered by sample planar transmission lines – coplanar waveguide (CPW) and microstrip line (MSL). The problem is that the effects on the dielectric and magnetic constant in these samples must be separated (to determine the degree of the ME effect), which has been performed in the paper. The additional circumstance is the possibility to determine the changes in the dielectric/magnetic loss tangent (or conductivity) of these samples; however, this is not possible to done with the needed accuracy in all considered cases. The paper considers also the description of the observed influences on the dielectric parameters of several artificial materials, already characterized in microwave range in our previous papers [33-35].

2. MATERIALS AND METHODS

2.1. *Characterization of Samples by Covering of 50-Ohms Coplanar Waveguides and Microstrip Lines*

Most of the artificial samples under interest in this paper have more or less expressed uni-axial anisotropy – different dielectric (and eventually magnetic) parameters in parallel and perpendicular directions regarding the sample surface [36]. This proven property (as considered in [32-35]) means that we can expect also anisotropy behaviour of the possible ME effect in these structures. Several papers consider such anisotropic ME effect [37-40]. Therefore, the proposed here method could have the possibilities to separate the dielectric (magnetic) parameters in different directions and to evaluate with enough selectivity and accuracy the possible observed ME effects in different directions.

We propose for characterization of ME effect to be applied the broadband transmission-line method, where the samples under test (SUT) cover 50-Ohms coplanar waveguides (CPW) or microstrip lines (MSL or tMSL) with different width of the strip conductors, as it has been shown in Fig. 1*a*. The dominant modes in the both structures, CPW and MSL, have high-frequency E and H fields placed high above the conductor layout and these fields penetrate into SUT. Thus, the SUT influences the additional insertion losses and insertion phase in the whole transmission lines; their frequency dependencies are representative measures of SUT dielectric and magnetic parameters, when a reliable extraction procedure has been performed (see the next section). In fact, the E fields in the CPW are orientated predominantly parallel to the waveguide substrate; therefore the CPW S parameters are influenced by the sample with anisotropy mainly through the pairs of parallel dielectric parameters (dielectric constant ε_{par} and dielectric loss tangent $\tan\delta_{\varepsilon_par}$) and the corresponding perpendicular magnetic components (magnetic constant μ_{perp} and magnetic loss tangent $\tan\delta_{\mu_perp}$) as it has been discussed in [32, 35]. MSL has a mixed distribution of E and H fields (neither pure parallel, nor pure perpendicular); therefore, the covered MSL allows extraction of a mixed (equivalent) value between the parallel and perpendicular dielectric and magnetic constants ($\varepsilon_{par,\ perp}$ and $\tan\delta_{\varepsilon_par,\ perp}$; $\mu_{par,\ perp}$ and $\tan\delta_{\mu_par,\ perp}$). A reliable determination of the dielectric and magnetic anisotropy is possible by resonance methods, e.g. by the authorship two-resonator method [40, 41], based on excitation of symmetrical TE_{0nm} and TM_{0n0} modes in cylinder resonators with SUT, which E fields are either parallel or perpendicular to the sample surface and E and H fields are mutually perpendicular. We will present data for the absolute measured anisotropic dielectric and magnetic parameters of the considered samples by the mentioned resonance methods in the next sections for corresponding materials.

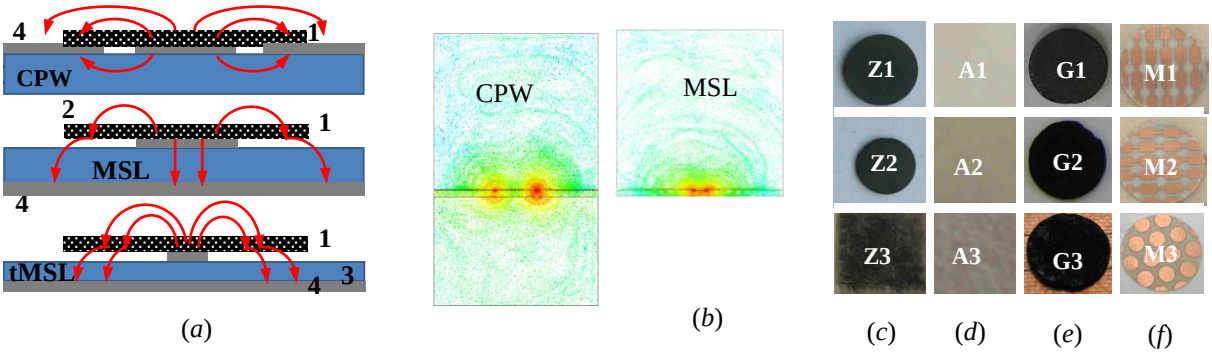


Fig. 1. Measurement structures and samples under test (SUT): (*a*) three covered by SUT planar lines: coplanar waveguide CPW (20 mils), microstrip line MSL (20 mils) and thin tMSL (10 mils); (*b*) 3D models of CPW and MSL (red colour – strong fields; green – medium fields; blue – weak fields); (*c*) Z-type hexaferrites (SUT) [32]: Z1 (SUT diameter d_S = 11.96; SUT heigth t_S = 1.2 mm); Z2 (d_S = 9.66; t_S = 0.67 mm); Z3 (t_S = 2-3 μm); (*d*) AAO [35]: A1 (with pure pores); A2 (semi-filled pores); A3 (pores, filled with Cu); (*e*) Carbon-content SUT [33]: G1 Spectral-pure Grapite (d_S = 8.05; t_S = 0.80, 1.00, 1.95 mm); G2 pressed Graphene (d_S = 8.40; t_S = 0.75 mm); G3 presses N-Graphene (d_S = 8.04; t_S = 0.90 mm); (*f*) Metamaterials with surface Cu inclusions [33, 34]: M1,2 "metasurfaces" placed perpendicularly or in parallel to the lines: non-symmetrical prizm unit cell 3*x*1.5 mm deposited on the both sides of substrate Arlon 25N (10 mils); M3 "meta-disks": symmetrical planar unit cell with disks of diameter 3 mm and distance between them 4 mm, single deposited on Arlon 25N (6 mils). *Legend*: 1 – SUT; 2 – E fileds of the dominant mode; 3 – substrate; 4 – metallization (17.5 μm)

The investigated in this paper selected artificial samples are presented in Fig. 1*b*,*c*,*d*,*e* (see the figure captions for details). They are: 1) Z-type hexaferrites $Sr_3Co_2Fe_{24}O_{41}$ (samples Z1,2,3) [32]; 2) porous anodic aluminium oxide Al_2O_3 (AAO), pure and with inclusions (samples A1,2,3) [35]; 3) Carbon-content pressed samples from Graphite, Graphene and N-doped Graphene (samples G1,2,3) [33] and 4) a set of different artificial metasamples with surface metal inclusions (samples M1,2,3) [34].

2.2. *Extraction of Sample Dielectric Parameters*

There are no enough accurate analytical approaches for extraction of dielectric and magnetic characteristics of covering SUT in CPW and MSL structures. In our case we performed simulations of well-constructed stylized 3-D models of the transmission-line planar structures (the procedure has been described in detail in [35]). Each structure has been solved in "driven-solution" option of the applied ANSYS®HFSS simulator and the insertion losses and phases of each CPW or MSL without and with SUT have been determined. The whole waveguide and SUT are placed in a relatively big "radiation box" in order to ensure enough room for the E/H fields above the line conductors to penetrate free in the SUT. The extraction procedure is as follows: 1) the waveguide structure is simulated without SUT; 2) then, the same structure with SUT is again simulated, tuning the values of equivalent dielectric constant ε_{eq} and equivalent dielectric loss tangent $\tan\delta_{\varepsilon_eq}$ of SUT until the simulated frequency dependencies of the additional phase and losses coincide with the corresponding measured dependencies. Proposed extraction procedure shows that the concrete parameters of the used planar lines, CPW and MSL, are not so important. However, there exists a measurement problem; usually an unavoidable air gap with effective thickness g_a appears between the sample bottom surface and the top CPW and MSL conductors due to different reasons: small curvatures, roughness, surface irregularities, etc. This effective gap can be evaluated by the help of known isotropic samples (e.g. PTFE; ε_r ~ 2.05; Polycarbonate, ε_r ~ 2.78). The obtained values are: g_a ~2±0.25 μm for MSL; g_a ~3.5±0.5 μm for tMSL and g_a ~15±2.5 μm for CPW.

Fig. 2 illustrates the proposed procedure for determination of the equivalent parameters of three types of AAO samples with different purity of the pores into the samples, considered in [34]. The procedure

allows determination of the equivalent dielectric parameters ε_{eq} and $\tan\delta_{\varepsilon_eq}$ of SUT; when these samples have incorporated metallic inclusions, the method allows also determination of the equivalent conductivity σ_{eq} of SUT (see figure captions for details). When SUT have also magnetic properties, a modified procedure (complimentary resonance and broadband methods) can be used for determination of both dielectric and magnetic properties with less accuracy (as in [32]). In this paper, the consider samples are with different characteristics. One type of samples (Z1,2,3) has simultaneously dielectric and magnetic properties, while another type (A1,2,3) – pure dielectric properties, but depending on the incorporated inclusions they may have magnetic properties or increased conductivity. Carbon-content samples (G1,2,3) have dielectric properties with relatively big conductivity. The last considered metasamples (M1,2,3) contain dielectric substrates with deposited on the surface metal inclusions. Therefore, the selected artificial samples for determination of ME effect in magnetic field cover wide ranges of material properties.

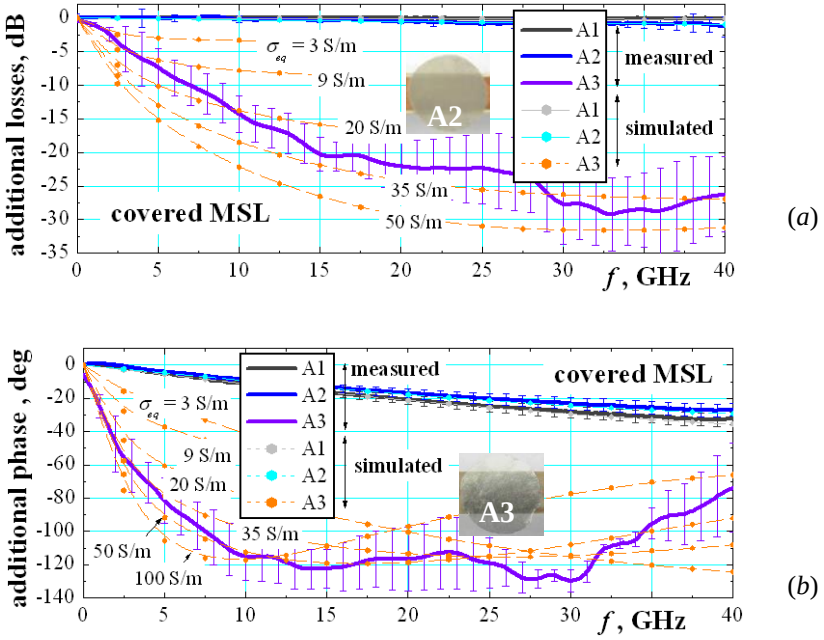


Fig. 2. Measured additional losses (*a*) and phase delay (*b*) in MSL transmission lines after covering by AOO samples (solid curves). Theoretical dependencies (dashed curves) are obtained by 3D simulations (HFSS) with dielectric parameters (anisotropy option): A1 (ε_{par} ~5.96; $\tan\delta_{\varepsilon_par}$ ~0.021; (ε_{perp} ~9.68; $\tan\delta_{\varepsilon_perp}$ ~0.0005); A2 (ε_{par} ~10.50; $\tan\delta_{\varepsilon_par}$ ~0.016; ε_{perp} ~2.78; $\tan\delta_{\varepsilon_perp}$ ~0.018); A3 (ε_{par} ~12.55; σ_{eq_par} ~20-50 S/m; ε_{perp} ~11.20; σ_{eq_perp} ~20-50 S/m;); and setting an effective air gap ~2.5 μm between SUT and conductor line

2.3. *Experimental Characterization of Magneto-Electric Efect in External Magnetic Fields*

The proposed magnetic systems are very suitable for applying of external dc magnetic field H_0 without strong parasitic influence on the microwave characteristics of the used measurement structures due to the proximity of the used magnets or conductors. Fig. 3 illustrates how this magnetic field H_0 (or the corresponding magnetic induction B_0) can be applied to magnetize the investigated SUT in two different directions – parallel and perpendicular to the sample. The external field H_0 could be produced either by pair of strong fixed permanent magnets or by electromagnet (for tunable H_0). The magnetic field can be applied either parallel (Fig. 3*a*) or perpendicularly to the SUT (Fig. 3*b*). This allows influence of the external dc magnetic field either over the parallel dielectric parameters of SUT, or over the perpendicular dielectric parameters. In the both cases the SUT is well pressed to the corresponding transmission line through a foam spacer with low values of the dielectric parameters (e.g. ε_f ~1.021 and $\tan\delta_{\varepsilon_f}$ ~0.00005) (Fig. 3*c*), which influence has been taken into account in the extraction procedure.

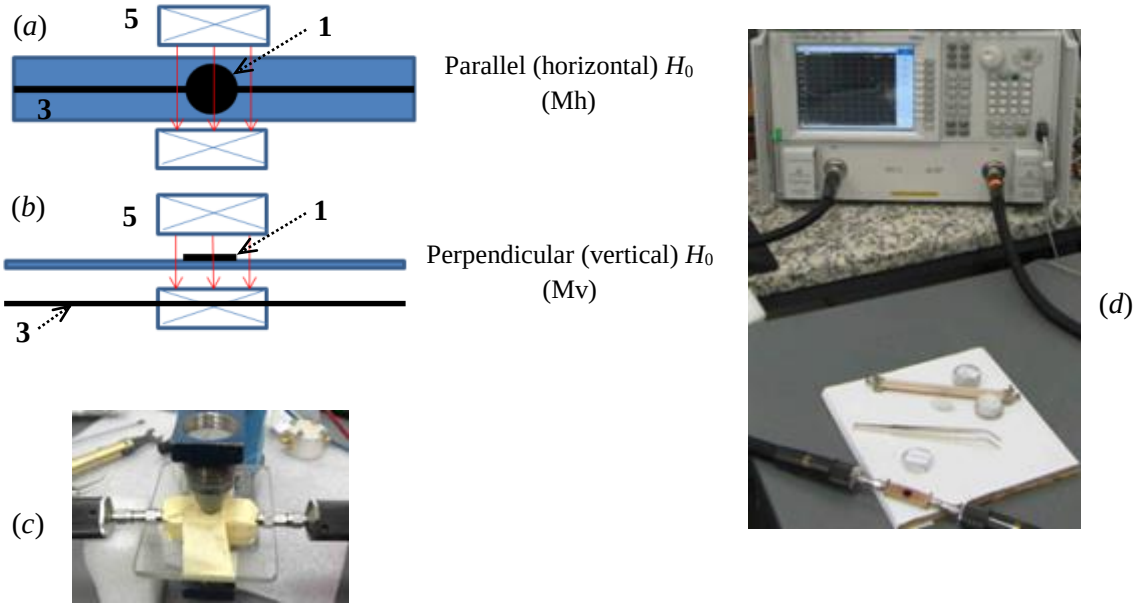


Fig. 3. Schematic view of the applied external dc magnetization of SUT in parallel/horizontal (*a*) and in perpendicular/vertical (*b*) direction to the sample; (*c*) electromagnet system with packaged SUT; (*d*) measurement set-up using vector network analyzer with CPW and SUT without electromagnet system. *Legend*: 1 – SUT; 3 – transmission-line substrate; 5 – electromagnet or pair of permanent magnets

The S parameters of the considered magnetized structures have been measured by a vector network analyzer VNA (Fig. 3*d*) in a wide frequency range 0.01-40 GHz. The procedure is as follows. First, the standardly calibrated VNA measures the vector transmitted S parameters of the pure CPW or MSL – S_{21} and angS_{21} (losses and phases). Due to the well matching of these 50-Ohms lines the measured S parameters can be saved in VNA memory and the new measured S parameters of the structures with SUT can be directly measured as additional losses and additional phases (as in Fig. 2). This allows direct characterization of the SUT influence over these parameters: bigger additional losses mean bigger SUT dielectric (and magnetic) loss tangent; while bigger phase delays – increased dielectric (and magnetic) constants of SUT (the nonlinear behaviour can be associated with appearance of increased conductivity of the samples, as in [33, 35] or with appearance of specific resonance effects due to the sample influence, as in [26, 27]). These data can be used for very informative characterization of the SUT, placed on the considered transmission line (as we have shown in [35] for AAO samples with inclusions, see also Fig. 2). Finally, the considered samples can be magnetized by the magnetic systems shown in Fig. 3*a*,*b*, which is the object of this paper. In this case, we can again save the measured S parameters of the transmission-line with sample without magnetization ($B_0 = 0$) and to determine the variations of the measured S_{21} and angS_{21} in increased dc magnetic field (see the next section). This simplified measurement procedure considerable facilitates the characterization of the eventual ME effect in the considered samples in two possible direction to the sample (Mh and Mv; see Fig. 3*a*,*b*).

3. RESULTS AND DISCUSSION

We performed a lot of measurements of the considered SUTs in different measurement structures (CPW, MSL or tMSL) and with two different orientation of the external magnetic field (parallel or perpendicular to SUT). Due to the lack of space, only part of the obtained results has been presented in this paper. These investigations could be considered as a first step to detect a magneto-electric effect in these samples without any preliminary information. Here the obtained effects are not bind with the

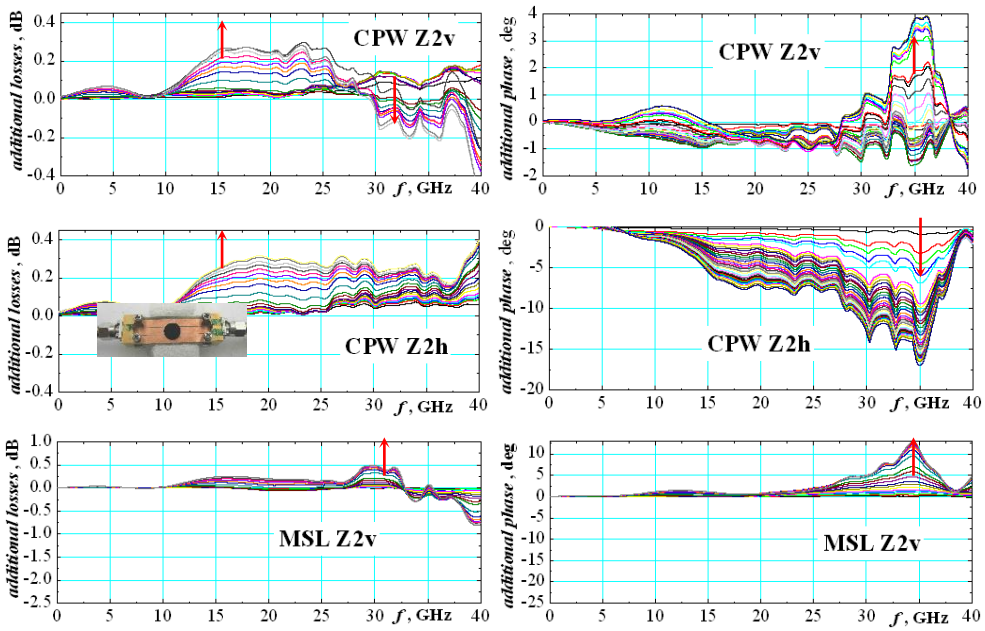
structure of the measured materials (this is a part of our future work). We simple detect of the possible effects and present some remarks about the reasons for the observed behaviour in each concrete case.

We applied three types of magnetic system for ensuring different intervals for the produced magnetic field. In one of the variants of the electromagnet system we produce relatively week magnetic field (magnetic induction B_0 between 0 and 0.133 T), while in other case – relatively stronger magnetic induction B_0 between 0 and 0.240 T). Finally, with the help of a pair of permanent magnets we can produce a relatively strong fixed magnetic induction up to ~0.4 T.

3.1. Magneto-Electric Effect in Z-type Hexaferrite Thick and Thin Samples

The considered Z-type hexaferrite $Sr_3Co_2Fe_{24}O_{41}$ multiferroic material (samples Z1,2,3) has been investigated in the microwave range (0.01-40 GHz) in our paper [32] for the first time. We obtained the following mean parameters of the considered material (sample Z2) in the frequency range 7-25 GHz: ε_{par} ~14.7, $\tan\delta_{\varepsilon_par}$ ~0.08; ε_{perp} ~ 9.30; $\tan\delta_{\varepsilon_perp}$ ~0.15 and μ_{par} ~0.75, $\tan\delta_{\mu_par}$ ~0.20; μ_{perp} ~0.98, $\tan\delta_{\mu_perp}$ ~0.10. We can see the strong anisotropy as for the dielectric parameters, as well as for the magnetic parameters due to the layered structure of the considered multiferroic material.

On this base, we performed a preliminary research of the variations of the additional losses and phases in the considered transmission-line structures due to the close presence of hexaferrite SUTs on their conductors in a tunable external magnetic field. The obtained results have been presented in Fig. 4 as a set of frequency dependences of the additional losses and additional phase in the used three structures CPW, MSL and tMSL for sample Z2 in parallel (marked as Z2h) and perpendicular (Z2v) direction to the sample. The zero values correspond for non-magnetized sample; therefore, the negative additional losses correspond to increased insertion losses and loss tangents in samples, while the positive ones – to decreased insertion losses in the whole sample; similarly: the negative additional phase delay corresponds to a dielectric (and/or magnetic) constant increase, while the negative ones – to a dielectric (and/or magnetic) constant decrease. Based on these rules, we can evaluate the possible ME effects in the considered multiferroic samples (see also data in Fig. 5 for the observed dependencies in the thicker disk sample Z1 and in the thin-layer sample Z3 in CPW structures).



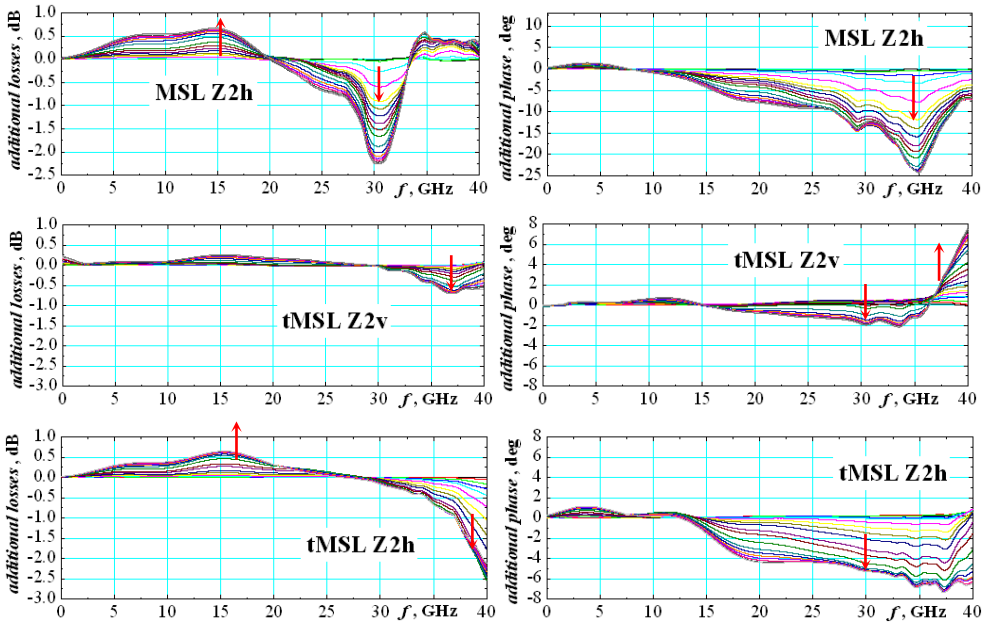


Fig. 4. Measured dependencies for the additional losses and phases in CPW, MSL and tMSL structures, caused by the magnetized disk sample Z2 in horizontal and vertical direction (magnetic induction in the interval B_0 = 0-0.133T), normalized to the values at B_0 = 0. The red arrows show direction for increasing of the external dc magnetic field

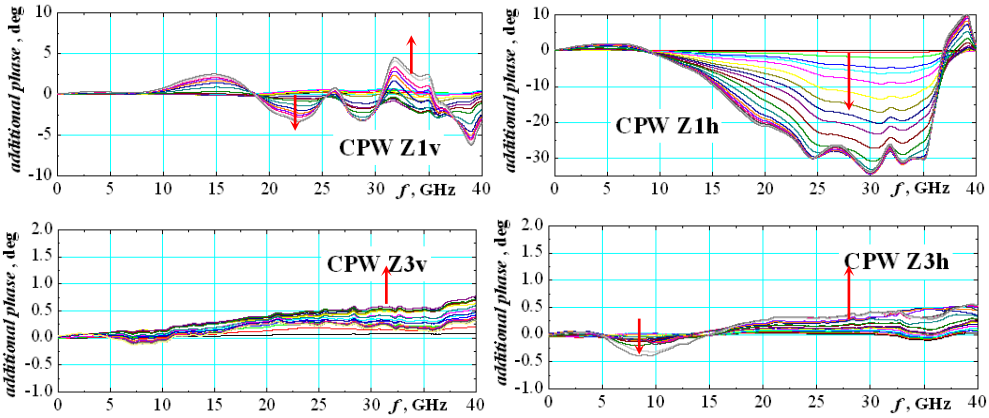


Fig. 5. The same as in Fig. 4 for thicker disk sample Z1 and for thin film Z3 on a ceramic carrier in CPW structure only (the dependencies for MSL and tMSL are similar)

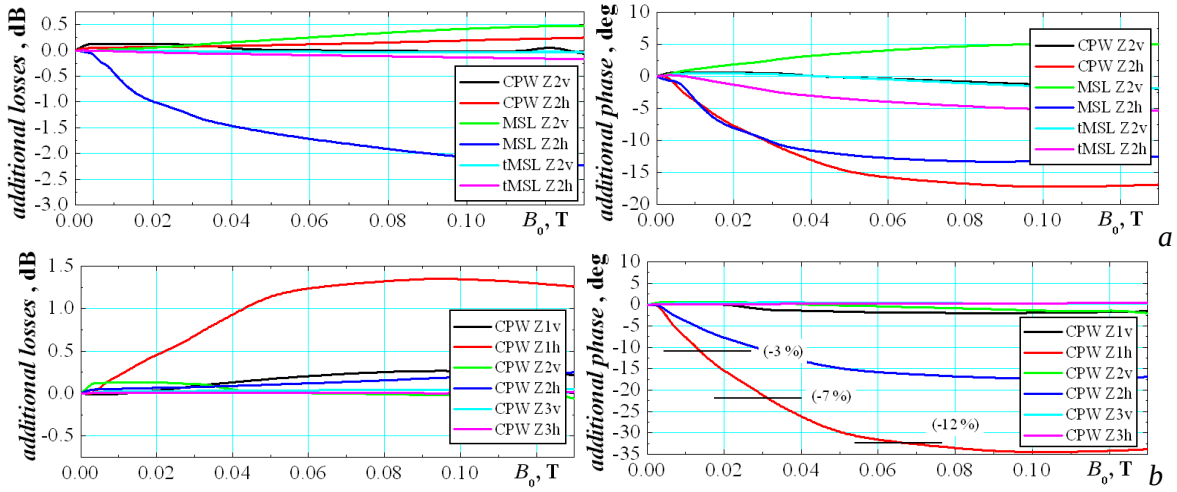


Fig. 6. Measured dependencies for the additional losses and phases in CPW, MSL and tMSL structures for sample Z2 (*a*) and only in CPW for all samples Z1,2,3 (*b*) versus the external horizontal and vertical magnetic induction in the interval B_0 = 0-0.133T at 30 GHz

Definitely, the external magnetic field influences the corresponding pairs of material parameters of the considered multiferoics, namely $\varepsilon_{par}/\mu_{perp}$; $\tan\delta_{\varepsilon_par}/\tan\delta_{\mu_perp}$ and/or $\varepsilon_{perp}/\mu_{par}$; $\tan\delta_{\varepsilon_perp}/\tan\delta_{\mu_par}$. The pair $\varepsilon_{par}/\mu_{perp}$ for all Z samples increases with the increase of the external horizontal magnetic field (because the phase delay increases in CPW structure, where the E fields are predominantly orientated in parallel direction, as it is shown in Fig. 1*a*). Very similar effects have been observed also for other planar structures MSL and tMSL. In the same time, the pair $\tan\delta_{\varepsilon_par}/\tan\delta_{\mu_perp}$ decreases in increasing external horizontal magnetic field (due to the observed positive additional losses in CPW structures; we will not discuss here the observed resonance effects for ~30 GHz for the losses and ~35 GHz for the phase). More clear dependencies are presented in Fig. 6 for the additional losses and phases at 30 GHz versus the applied magnetic field. Here the discussed above effects are more visible. On the contrary, the pair $\varepsilon_{perp}/\mu_{par}$ slightly decreases in vertical external magnetic field at 30-40 GHz; this dependence can be observed for MSL and tMSL structures in Fig. 4 or Fig. 6. The presented in Fig.6*b* %-values on the phase delay dependence in horizontal magnetic field illustrate the relatively big decrease of the product ε_{par} *x* μ_{perp} in the CPW structure, compared with the negligible small changes for the product ε_{perp} *x* μ_{par} in vertical magnetic field.

However, from the results shown above we cannot conclude if the applied horizontal magnetic field influences mainly the dielectric constants (ε_{par}) of the considered Z samples (and eventually $\tan\delta_{\varepsilon_par}$) or the observed effects are connected only with magnetic constant (μ_{perp}) variations (and $\tan\delta_{\mu_perp}$), or we can observe both effects? For this purpose, we performed classical perturbation measurements in rectangular resonators in the X band of small prisms (1.22 *x* 2.07 *x* 10.16 mm) made from sample Z1. In such structures, a set of resonances of the dominant mode $TE(H)_{10p}$ (p = 1, 2, 3, 4, 5, 6,…) can be observed. Fig. 7 presents the resonance behaviour of two modes H_{103} and H_{104} in horizontal and vertical external fields according the prism sample plane of rectangular resonator in the X band (8-12 GHz) (we have also perturbation measurements in the Ku, K and Ka bands in the frequency range 12-40 GHz; but they are not shown here). A common property of the exited resonances is the observation of maximums of the vertical E fields for modes with odd values of index p (but with expressed magnitude of the horizontal H field), and maximums of the H field (with zero E fields) for modes with even p values (see the illustrations in Fig. 8 of the simulated E- and H-field distributions of modes H_{103} and H_{104} in rectangular resonator with prism sample in the resonator centre). From these dependencies we can extract the variations in horizontal external dc magnetic field as for the dielectric constant, as well as for the magnetic constant of the considered multiferroic samples and these variations can be well separated (we don't consider in this paper the variations of the dielectric and magnetic loss tangents in external magnetic field; this is an object of our next publications).

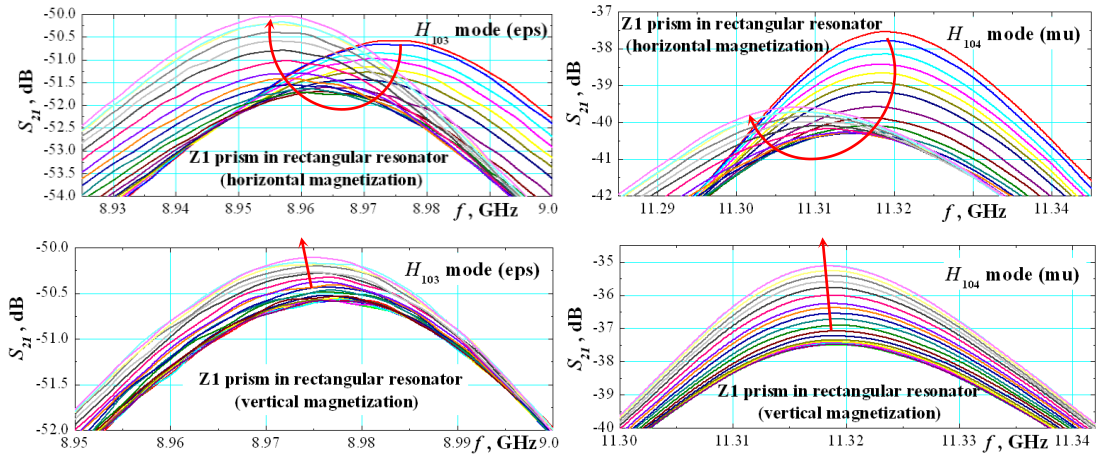


Fig. 7. Resonance curves of different H_{10p} modes (p = 1, 2, 3, 4, 5, 6…; in this case p = 3 or 4) in rectangular resonators (WR90; dimensions: 64.95 *x* 22.86 *x* 10.16 mm) with Z-feroic prisms (1.22 *x* 2.07 *x* 10.16 mm) made from the multi-ferroic sample Z1 placed in the resonator centre. These resonances have been influenced mainly by the dielectric (marked as eps) or by the magnetic (mu) constants of the sample in horizontal (first row) and vertical (second row) magnetic field B_0 = 0-1.33 kOe (the red arrows show the directions for B_0 increase).

Let's transform the observed resonance frequencies (Fig. 7) into dependencies of the frequency shifts of the resonances in external magnetic field – see Fig. 9*b*; they have been compared with the dependencies of the phase delays in the same disk sample Z1 on CPW versus the magnetic induction in both horizontal/vertical directions – Fig. 9*a*. The conclusion is that the influence of the applied horizontal induction B_0 is 5-6 times bigger, which clearly indicates the existence of expressed anisotropy of the measured ME effects. Thus, from the resonance frequencies' shifts of the excited TE_{10p} modes, we can separately extract the variation of the equivalent magnetic μ_{eq} (p = 2, 4, 6) and dielectric ε_{eq} (p = 1, 3, 5) constants of the considered multiferroic sample in a given frequency range. The procedure for the numerical extraction of the equivalent material parameters μ_{eq} and ε_{eq} is as follows. First of all, the resonator without sample has to be simulated for each resonance to determine the right equivalent resonator length and to achieve at least 1-2-% coincidence between the measured and simulated resonance frequencies for each mode. Then, the simulations of the resonance structures with SUT for modes with even values of the index p (= 2, 4, 6) ensure determination of the values of μ_{eq} at the corresponding frequency (the E-fields are ~0 in the resonator centre for these modes and any introduced ε_{eq} value don't change the resonance frequency for such thin prism samples). After determination of μ_{eq}, this value must be introduced in the 3D model of the resonator with SUT for the neighbor mode with odd index p (= 1, 3, 5); this allows determination of the right ε_{eq} value. Fig. 9*b* presents two dependencies of the resonance shifts in horizontal magnetic field: one curve for mode H_{104}, which depends only from the variations of μ_{eq}, and another curve for mode H_{103}, which depends on the combination of μ_{eq} and ε_{eq}. The analysis of the results in Fig. 9*b* allows us to conclude that the smaller external magnetic fields (B_0 ≤ 0.04 T) influence stronger the dielectric constant ε_{eq}, while the stronger fields (H_0 > 0.08 kOe) – the magnetic constant μ_{eq}, where ε_{eq} variations show a saturation. These conclusions have been confirmed by the broadband CPW measurements; see dependencies in Fig. 9*a*, where a 10-12 % variation of the material constants can be achieved, which is enough to conclude that ME effect in these multiferoics sample fully exists in the microwave range. Our investigations in this area are in progress.

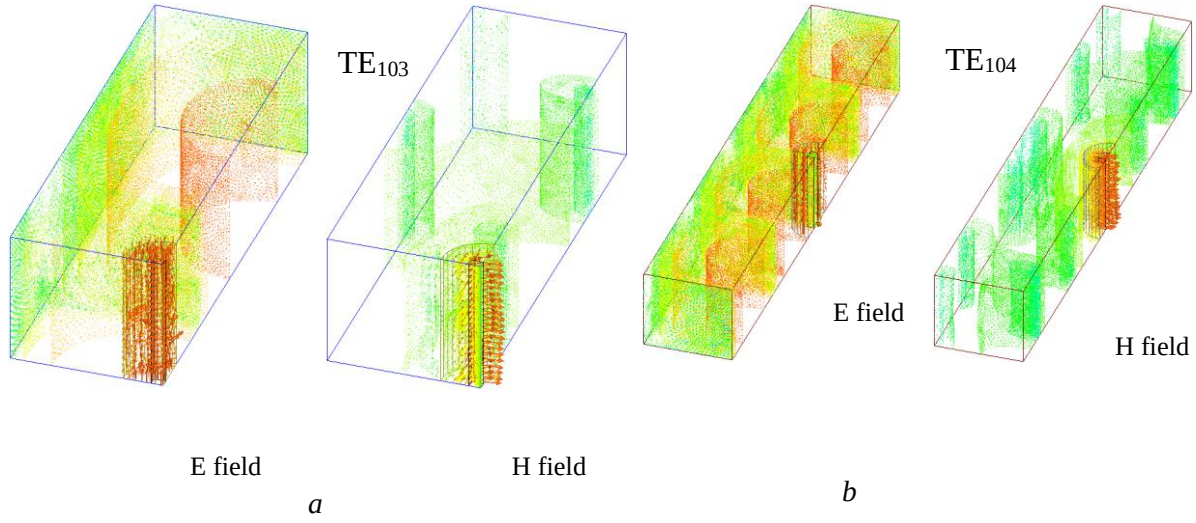


Fig. 8. (*a*) Variations of the additional phase in CPW structure with multi-ferroic disk sample Z1 at 30 GHz v/s magnetic field H_0; (*b*) shift of resonance frequency of modes TE_{103} and TE_{104} due to magnetized multiferroic prism made from sample Z1 in external magnetic field B_0 = 0-0.133 kOe, normalized to values at B_0 = 0.

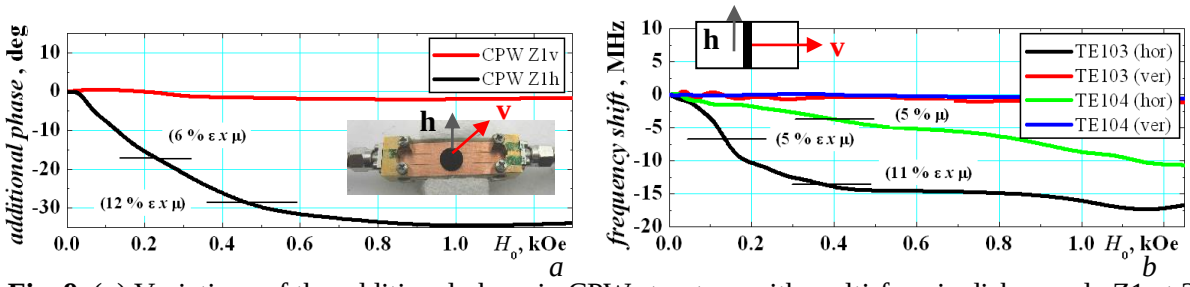


Fig. 9. (*a*) Variations of the additional phase in CPW structure with multi-ferroic disk sample Z1 at 30 GHz v/s magnetic field H_0; (*b*) shift of resonance frequency of modes TE_{103} and TE_{104} due to magnetized multiferroic prism made from sample Z1 in external magnetic field B_0 = 0-0.133 kOe, normalized to values at B_0 = 0.

3.2. Magneto-Electric Effect in Anodic Aluminium Oxide with Metal Inclusions

Very surprising is the behaviour of pure dielectric AAO samples in external magnetic fields – see data in Fig. 8.

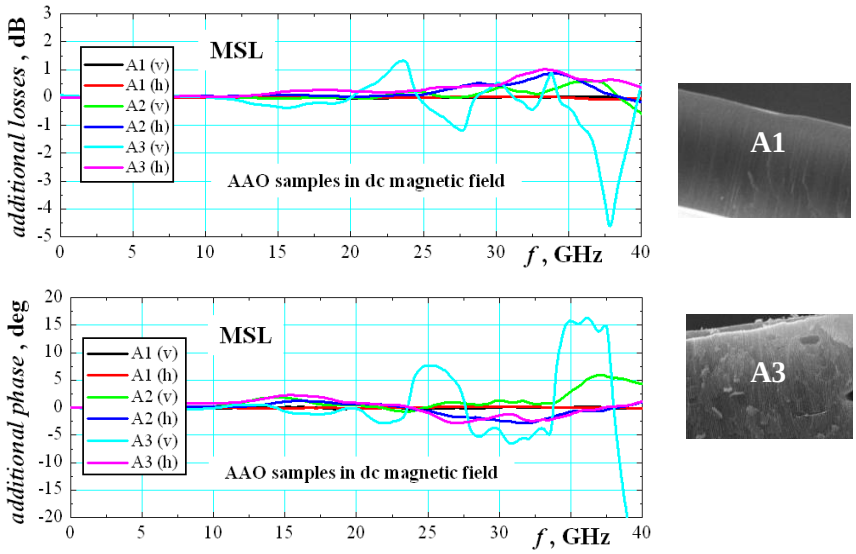


Fig. 10. Measured dependencies for the additional losses and phases in MSL structure, caused by magnetized AAO samples with different purity in horizontal and vertical fixed magnetic induction 0.4T. Insets show the pores' purity in samples A1 and A3 (pore diameter ~35 nm) [35].

If the samples have pores without inclusions (A1), we cannot detect any changes in external magnetic fields. For samples with nano-inclusions from iron magnetite Fe_3O_4, which appears during the fabrication process (A2 and A3), the external vertical magnetic field (parallel to the pores) caused changes as in the additional losses, as well as in the additional phase (mainly for sample A3 with high degree of metallic inclusions; compare with the dependencies in Fig. 2). The simulations show that this effect can be related to observation of changes in the equivalent conductivity of the AAO samples; the equivalent dielectric constant ε_{eq} practically remains constant.

3.3. Magneto-Electric Effect in Carbon-Content Samples

In this paper, we present also preliminary data for variation of the frequency behaviour of the dielectric parameters and conductivity of Carbon-content samples (pressed Graphite, Graphene and N-Graphene disks) – Fig. 11. The influence of the external magnetic field on the additional losses is small; however, the positive changes of the additional phase in vertical magnetic field show that the dielectric constant (probably the perpendicular value) decreases in magnetic field due to the layered sample structure.

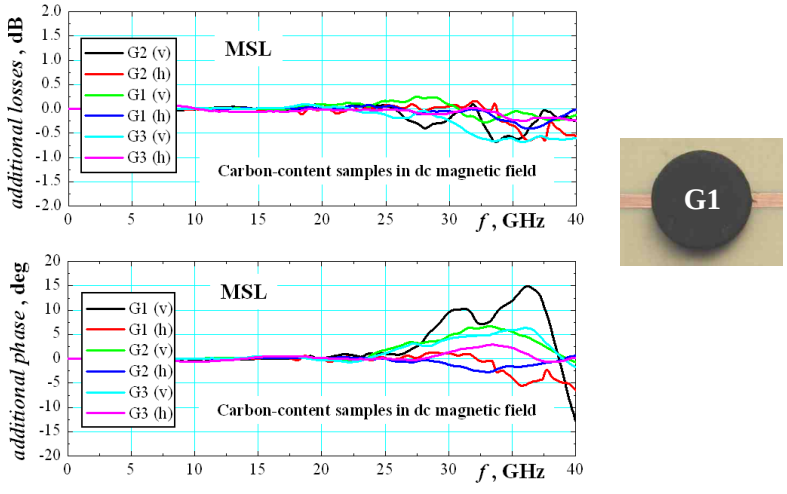


Fig. 11. Measured dependencies for the additional losses and phases in MSL structure, caused by magnetized Carbon-content samples (pressed Graphite, Graphene and N-Grafene disks) in horizontal and vertical direction (fixed magnetic induction 0.4T) [33].

3.4. Magneto-Electric Effect in Metamaterials with Metal Surface Inclusions

The last example relates to investigation of the external magnetic field influence on some metamaterial surface, considered in [33, 34]. These materials consist of ordinary reinforced substrates with deposited metal inclusions on their surfaces.

The sample M3 has a symmetrical set of metal disks and shows behaviour as an artificial dielectric with increased dielectric constant (from 3.5 up to 10-15 depending on disks sizes and distance between them [33]). In magnetic field these artificial dielectrics don't show any measurable changes.

Similar effect (no visible changes in external magnetic field) we observe also for an especially designed metasurface (sample M2), when the electric fields of the used transmission line structure are orientated perpendicularly to the unit cells of the metal prisms. However, when the electric field of the dominant mode in the MSL structure are orientated along the prism set (sample M1), the measured dielectric constant show strongly negative equivalent dielectric constants in the frequency range 20-28 GHz [33]. From the dependencies in Fig. 12 we can see also a relatively big influence of the external dc magnetic field in the both directions exactly in the frequency range 20-28 GHz, where the metasurface has been designed to "work" (strong anisotropy of the perpendicular and parallel dielectric constants). The variations correspond to a decreasing of the equivalent dielectric constant ε_{eq} in horizontal dc magnetic field, and to an increasing of ε_{eq} in vertical dc magnetic field). The other coincidence can be observed with the measured equivalent conductivity σ_{eq} of this metasurface, presented in [43].

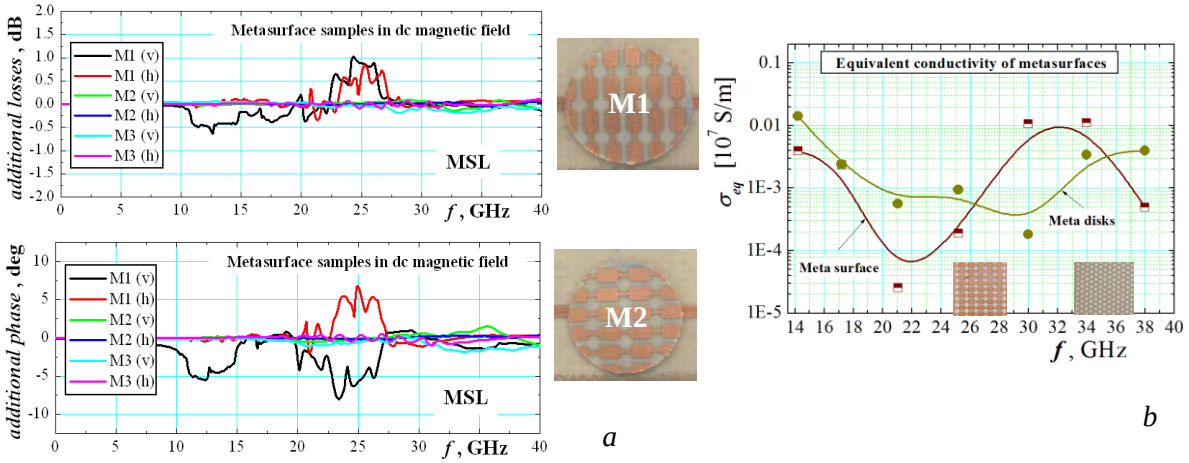


Fig. 12. (*a*) Measured dependencies for the additional losses and phases in MSL structure, caused by magnetized metamaterials with metal inclusions (see the insets and pictures in Fig. 1*f*) in horizontal and vertical direction (fixed magnetic induction 0.4T); (*b*) measured equivalent conductivity of the same samples [43].

5. CONCLUSIONS

The presented research is very interesting from the point of view of the possibility to detect and even to evaluate quantitatively the magneto-electric effects in some composite structures with different behaviour in the microwave range. We manage to detect changes in the equivalent dielectric constant in some of these samples in the frequency range up to 40 GHz in dependence of the orientation of the external magnetic field and its magnitude. In some cases, we can determine the absolute values of the changes in the dielectric constant and to separate these changes from the magnetic constant variations in the same magnetic fields. Of course, it is important also the measure the opposite effects – the changes of the equivalent magnetic constant in external electric dc fields with magnitude of several kV/cm (for example, the measurement structure based on CPW allows this possibility).

These investigations have a concrete aim to perform acceptable tunable structures (by external dc magnetic or electric fields) for different antenna and RF applications, mainly for tunable phase shifters and/or delay lines for reliable beamforming in the new generation of antenna arrays.

ACKNOWLEDGMENT

The method development has been supported by the National Research Fund in Bulgaria under grant #DN07/15. The authors would like to thank to Dr. T. Koutzarova and Dr. S. Kolev from Institute of Electronic of Bulgarian Academy of Science for the Z-type hexaferrite samples, to Prof. V. Videkov and Dr. B. Tzaneva from Technical University of Sofia for the AAO samples, and to Prof. E. Tatarova from Instituto Superior Technico (IST) Lisbon for the Graphene and N-Graphene samples.

REFERENCES

1. Nana C-W, Bichurin M I, Dongb S, Viehland D, Srinivasanm G 2008, "Multiferroic magneto-electric composites: Historical perspective, status, and future directions," *J. Appl. Phys.* 103, 031101-1-35
2. Srinivasan G 2010, "Magnetoelectric Composites," *Annu. Rev. Mater. Res.* 40:153–78, 2010.40:153-178
3. Tiwari S, Vitta S 2018, "Magnetoelectric and magnetodielectric coupling and microwave resonator characteristics of $Ba_{0.5}Sr_{0.5}Nb_2O_6$/ $CoCr_{0.4}Fe_{1.6}O_4$ multiferroic composite," *Scientific Reports*, 8:11619 DOI:10.1038/s41598-018-30132-2
4. Iguchi Y, Nii Y, Onose Y, "Magnetoelectrical control of nonreciprocal microwave response in a multiferroic helimagnet," *Nature Communications*, 8:15252, DOI: 10.1038/ncomms15252
5. Zhang J, Kang Y, Gao Y, and Weng G J 2019, "Experimental Investigation of the Magnetoelectric Effect in NdFeB-Driven A-Line Shape Terfenol-D/PZT-5A Structures", *Materials*, 12, 1055; doi:10.3390/ma12071055 www.mdpi.com/journal/materials
6. Srinivasan G, and Fetisov Y K 2006, "Microwave Magnetoelectric Effects and Signal Processing Devices," *Integrated Ferroelectrics*, Taylor&Francis Group, 83:1, pp. 89-98 DOI: 10.1080/10584580600949105
7. Bichurin M, Petrov R, Leontiev V, Semenov G, and Sokolov O 2017, "Magnetoelectric Current Sensors," *Sensors*, 17, 1271; doi:10.3390/s17061271 www.mdpi.com/journal/sensors
8. Eerenstein W, Mathur N D, Scott J F 2006, "Multiferroic and magnetoelectric materials," *Nature*, vol. 442, 05023
9. Pettiford C I 2008, "Novel Microwave Magnetic and Magnetoelectric Composite Materials and Devices", PhD Thesis, Department of Electrical and Computer Engineering, Northeastern University Boston, Massachusetts
10. Rožič B *et al*. 2012, "Magnetoelectric effect in soft composite materials," *Proceedings of ISAF-ECAPD-PFM 2012*, Aveiro, pp. 1-4, doi: 10.1109/ISAF.2012.6297753
11. Zhou Y, Maurya D, Yan Y, Srinivasan G, Quandt E, and Priya S 2015, "Self-Biased Magneto-electric Composites: An Overview and Future Perspectives," *Energy Harvesting and Systems*, July 2015; DOI 10.1515/ehs-2015-0003
12. Bala K, Kotnala R K, Negi N S 2016, "Magnetically tunable dielectric, impedance and magneto-electric response in MnFe2O4/(Pb1−xSrx)TiO3 composites thin films," *Journal of Magnetism and Magnetic Materials*, DOI: 10.1016/j.jmmm.2016.10.059

13. Yan Y, Zhou Y, and Priyab S 2014, "Enhanced magnetoelectric effect in longitudinal-longitudinal mode laminate with cofired interdigitated electrodes," *Applied Physics Letters*, 104, 032911 [http://dx.doi.org/10.1063/1.4862183]; pp. 032911-1 032911-5
14. Amirov A, Baraban I, Panina L, and Rodionova V 2020, "Direct Magnetoelectric Effect in a Sandwich Structure of PZT and Magnetostrictive Amorphous Microwires," *Materials*, 13, 916; doi:10.3390/ma13040916 www.mdpi.com/journal/materials
15. Maksymov I S and Kostylev M 2013, "Impact of conducting nonmagnetic layers on the magnetization dynamics in thin-film magnetic nanostructures," *J. Appl. Phys*. 113, 043927; doi: 10.1063/1.4789812
16. Zhou P, Popov M A, Liu Y, Bidthanapally R, Filippov D A, Zhang T, Qi Y, Shah P J, Howe B M, McConney M E, Luo Y, Sreenivasulu G, Srinivasan G, and Page M R 2019, "Converse magnetoelectric effects in composites of liquid phase epitaxy grown nickel zinc ferrite films and lead zirconate titanate: Studies on the influence of ferrite film parameters," *Physical Review Materials*, 3, 044403; DOI: 10.1103/PhysRevMaterials.3.044403
17. Zhou P, Singh A V, Li Z, Popov M A, Liu Y, Filippov A, Zhang T, Zhang W, Shah P J, Howe B M, McConney M E, Srinivasan G, Page M R, and Gupta A 2019, "Magneto-Electric Interactions in Composites of Ferrite Films on Lattice-Matched Substrates and Ferroelectrics", *Phys. Rev. Applied*, 11, 054045
18. Sudersan S and Arockiarajan A 2019, "Finite Element Formulation for Analysis of Unsymmetric Magnetoelectric Laminated Plates," *Proc. SPIE 10967, Active and Passive Smart Structures and Integrated Systems XIII*, 109671W; https://doi.org/10.1117/12.2514481
19. Kitagawa Y, Hiraoka Y, Honda T *et al.* 2010, "Low-field magnetoelectric effect at room temperature." *Nature Mater* 9**,** pp. 797–802; https://doi.org/10.1038/nmat2826
20. Ebnabbasi K, Chen Y, Geiler A, Harris V, and Vittoria C 2012, "Magneto-electric effects on Sr Z-type hexaferrite at room temperature", *J. of App. Phys*., 111, doi: 10.1063/1.3678588
21. Wang X, Su Z, Sokolov A, Hu B, Andalib P, Chen Y, and Harris V G 2014, „Giant magneto-resistance due to magnetoelectric currents in Sr3Co2Fe24O41 hexaferrites", *App. Phys. Lett.*, 105, 112408,
22. Palneedi H, Annapureddy V, Priya S, and Ryu J 2016, "Status and Perspectives of Multiferroic Magnetoelectric Composite Materials and Applications," *Actuators*, 5, 9; doi:10.3390/act5010009
23. Sun N X, Srinivasan G 2012, "Voltage Control of Magnetism in Multiferroic Heterostructures and Devices," *SPIN*, vol. 2, No. 3 1240004; DOI: 10.1142/S2010324712400048
24. Koutzarova T, Ghelev Ch, Peneva P, Georgieva B, Kolev S, Vertruyen B, and Closset R 2018, "Hexaferrite multiferroics: from bulk to thick films," *IOP Conf. Series: Journal of Physics: Conf. Series* 992 012058; doi :10.1088/1742-6596/992/1/012058
25. El Fellahi A, Mazzamurro A, Gerbedoen J C, Dusch Y, Matar O B, Pernod P, Talbi A, and Tiercelin N 2018, "Miniaturized Coplanar Waveguide for Nanostructured Magnetostrictive Multilayer Characterization", *MDPI Proceedings*, 2, 851; doi:10.3390/proceedings2130851
26. Głowiński H., Schmidt M., Gościańska I., Dubowik J., and Ansermet J-Ph. 2014, "Coplanar waveguide based ferromagnetic resonance in ultrathin film magnetic nanostructures: impact of conducting layers," *arXiv:1402.5844* [cond-mat.mes-hall]; DOI: 10.1063/1.4891734
27. Khivintsev Y. V., Reisman L., Lovejoy J., Adam R. Schneider C. M., Camley R. E., and Celinski Z. J. 2010, "Spin wave resonance excitation in ferromagnetic films using planar waveguide structures," *J. Appl. Phys.* 108, 023907; pp. 023907-2/6
28. Tatarenko A S and Bichurin M I 2012, "Microwave Magnetoelectric Devices", *Advances in Condensed Matter Physics*, Hindawi Publishing Corporation, ID 286562, doi:10.1155/2012/286562

29. Tatarenko A S, Snisarenko D V, Bichurin M I 2017, "Modeling of Magneto-Electric Microwave Devices", *Facta Universitatis, Ser. Electronics and Energetics*, v. 30, No.3, Sept., pp.285-293 DOI: 10.2298/FUEE1703285T

30. Tatarenko A., Sokolov O., Ivanov S., Bichurin M., and Wang Y. 2019, "Microwave magneto-electric effect in structures based on ferromagnetic metals," *ITM Web of Conferences* 30, https://doi.org/10.1051/itmconf /201930; CriMiCo'2019 7013 07013

31. Kalarickal S. S., Krivosik P., Wu M., Patton C. E., Schneider M. L., Kabos P., Silva T. J., Nibarger J. P. 2006, "Ferromagnetic resonance linewidth in metallic thin films: Comparison of measurement methods," *J. Appl. Phys.* 99, 093909; pp. 093909-1 093909-7

32. Dankov P, Kolev S, Koutzarova T 2020, "Dielectric and Magnetic Properties of Hexaferrite $Sr_3Co_2Fe_{24}O_{41}$ Thin Samples in the Microwave Range", *VIET2019*, Sozopol, Bulgaria; *IOP Conf. Series: Journal of Physics: Conf. Series* 1492 012048; doi:10.1088/1742-6596/1492/1/012048

33. Dankov P I 2019, "Characterization of Dielectric Properties of Conductive Materials by Coplanar Waveguide Method", *IEEE 19th Mediterranean Microwave Symposium*, Tunisia, Nov. (online available)

34. Dankov P I 2019, "Experimental Characterization of Positive and Negative Dielectric Constants and Artificial Anisotropy of Metamaterials in the Microwave Range", *Journal of Physics: Conf. Series*, IOP Publishing (in print)

35. Dankov P, Tzaneva B, Videkov V 2019, "Microwave Characteristics of Thin Al_2O_3 Membranes as Metasamples for Optical Applications," *Proc. of SPIE* 11332, Int. Conference on Quantum, Nonlinear, and Nanophotonics (ICQNN 2019), 1133203; doi: 10.1117/12.255189

36. Dankov P I 2020, "Material Characterization in the Microwave Range, When the Materials Become Composite, Reinforced, 3D-Printed, Artificially Mixed, Nanomaterials and Metamaterials (review paper), *Forum for Electromagnetic Research Methods and Application Technologies (FERMAT)*, accepted for publication

37. Fetisov L Y, Saveliev D V, Chashin D V et al. (2019), "Anisotropic Magnetoelectric Effect in a Magnetostrictive Fiber Composite –Piezoelectric Plate Structure," *Phys. Metals Metallogr*. 120, pp. 1304-1308; https://doi.org/10.1134/S0031918X19130052

38. Fetisov Y, Chashin D, Saveliev D, Fetisov L, and Shamonin M 2019, "Anisotropic Magnetoelectric Effect in a Planar Heterostructure Comprising Piezoelectric Ceramics and Magnetostrictive Fibrous Composite," *Materials*, 12(19), 3228; https://doi.org/10.3390/ma12193228

39. Vidala J V, Timopheeva A A, Kholkin A L, Sobolevac N A 2015, "Anisotropy of the magnetoelectric effect in tri-layered composites based on single-crystalline piezoelectrics," Vacuum, vol. 122, Part B, December, pp 286-292, https://doi.org/10.1016/j.vacuum.2015.06.022

40. Wang Y, Zhang N, Berakdar J, and Jia C 2013, "Tunable anisotropic magnetoelectric effect in helimagnetic tunnel junctions with interface Rashba spin-orbit interaction," *Appl. Phys. Lett.* 103, 052903; https://doi.org/10.1063/1.4816756

41. Dankov P 2006, "Two-resonator method for measurement of dielectric anisotropy in multilayer samples", *IEEE Trans. on Microwave Theory and Techniques*, v. 54, no. 4, July, pp. 1534-1544, DOI: 10.1109/TMTT.2006.871247

42. Dankov P I 2010, "Dielectric Anisotropy of Modern Microwave Substrates", Ch. 4 in "Microwave and Millimeter Wave Technologies from Photonic Bandgap Devices to Antenna and Applications", ed. I. Minin, In-Tech Publ. , ISBN 978-953-7619-66-4

43. Dankov P, Traykov R, Peshlov V, and Kamenopolski S 2018, "Equivalent Conductivity Characterization of Silver-Coated Plastic Antenna Components in Ku, K and Ka Bands," *Asia-Pacific Micro-wave Conference APMC2018*, November 6-9 2018, Kyoto, Japan (online available: IEEE Xplore)